Journal of Fluorine Chemistry 132 (2011) 529–535

Contents lists available at ScienceDirect

Journal of Fluorine Chemistry

journal homepage: www.elsevier.com/locate/fluor

Defluoridation kinetics of 200 °C calcined bauxite, gypsum, and magnesite and breakthrough characteristics of their composite filter

Bernard Thole *

Ngurdoto Defluoridation Research Station, P.O. Box 3020, Usa River, Arusha, Tanzania

ARTICLE INFO

Article history:
Received 11 March 2011
Received in revised form 7 May 2011
Accepted 16 May 2011
Available online 25 May 2011

Keywords:
Bauxite
Defluoridation
Fluorosis
Gypsum
Magnesite

ABSTRACT

Reaction kinetics and breakthrough characteristics in water defluoridation were studied through experiments with 200 °C-calcined bauxite, gypsum and magnesite and their composite filter. The aim was to determine defluoridation potential of a composite filter of the three locally sourced natural materials in contribution towards fluorosis mitigation. The materials were crushed and sieved to particle sizes of 1.2–1.4 mm diameter, and then heat-treated at 200 °C for 2 h. Their defluoridation capacities and reaction kinetics were determined in batch. A composite was then prepared in the ratio of the loading capacities. Breakthrough characteristics were experimented on in fixed bed through bed depth service time (BDST) design model, empty bed residence time (EBRT) optimisation model and the two parameter-logistics (2-PL) model. Mean loading capacities of 5.6, 3.4 and 1.7 mg F^-/g were obtained for bauxite, gypsum and magnesite, respectively. Loading capacities decreased, while sorption percentages increased, with increase in dose level. Second order kinetics observed had rate constants 4.07×10^{-2}, 1.87×10^{-2}, 1.59×10^{-2} g mg^{-1} min^{-1} for bauxite, gypsum and magnesite, respectively. Composites, bauxite and gypsum decreased, while magnesite increased water pH. Time at 50% breakthrough (τ) obtained experimentally compared well with τ obtained through the two-parameter logistics model indicating good fitness of data to the model. Greater doses obtained higher breakthrough times that were, 120, 210, 255 and 360 min for 45, 75, 120 and 150 g, respectively. Critical bed depth (Z_o), 7.71 cm and an operating line, $\hbar = 4 \times 10^{-4}\delta - 0.0757\delta + 4.86$ ($\hbar$ = adsorbent exhaustion rate, δ = EBRT) were obtained. The water quality was within recommended quality limits for pH, apparent colour, hardness, and residual concentrations of SO_4^{2-}, Cl^-, Fe^{2+}, and Al^{3+} in fixed bed. The research showed that a composite filter of the three materials, prepared in the ratio of their loading capacities and calcined at 200 °C, is a potential defluoridating filter in fixed bed configuration.

1. Introduction

1.1. Water defluoridation

Research work on removal of fluoride from water, referred to as water defluoridation, has resulted into the development of a number of technologies over the years. The well known techniques include precipitation, adsorption, ion exchange and reverse osmosis [1]. Adsorption is greatly employed in many high fluoride areas because it is cost-effective, versatile and easy to operate [2]. The competitiveness of adsorption to other techniques has led to increasing research interests in adsorption with various synthetic and natural materials world over. Research has shown that alkaline earth metal hydroxides/oxides have strong affinity for fluoride [2]. This renders them potential fluoride-adsorbents. Synthetic alkaline earth metals, however, are usually expensive as such their use in the treatment of drinking water is restricted. Naturally occurring alkaline earth metal salts such as magnesite and gypsum, offer potential alternatives for fluoride sorption in adsorption. Singano [3] demonstrated that use of magnesite in water defluoridation increases the water pH to 10. Gypsum was noted to introduce Ca and SO_4^{2-} in the water [4]. Bauxite and clays raise the turbidity and colour of the water [4,5]. Preliminary results showed that calcined gypsum and bauxite were reducing water pH [5]. These outcomes motivated search for possible combinations of the three materials that could maintain water pH within recommended WHO pH limits when employed in defluoridation. The current research investigated fluoride sorption in batch and fixed bed with bauxite, Al_2O_3, gypsum, magnesite and their composite calcined at 200 °C. The aim was to determine the possibility of developing a composite filter of the three materials that can effectively remove fluoride from water without altering the water quality beyond recommended WHO quality standards. The use of naturally occurring bauxite, gypsum and magnesite ensures availability of

* Fax: +255 272 553 540; mobile: +255 789 333 124.
E-mail address: tholebernard@hotmail.com.

0022-1139/$ – see front matter © 2011 Elsevier B.V. All rights reserved.
doi:10.1016/j.jfluchem.2011.05.016

adsorbent material thus mitigates the cost limitation of such a technology when synthetic metal oxides have to be purchased.

1.2. Research on fluoride sorption

Fluorine is found in nature as fluoride salts. Fluoride ions beneficial effects to dental and skeletal health when taken in quantities below 1.0 mg/l in potable water [6–8]. Quantities beyond 1.5 mg/l result in dental fluorosis, mottling and browning of teeth, while quantities around 10 mg/l cause crippling fluorosis characterised by deformities of bones [9–11]. The effects of fluoride on human health, and consequent desire to overcome the problem of excessive fluoride in drinking water, has resulted into water defluoridation being tried with a variety of materials. Among adsorbent materials that have been researched on are; bone charcoal, activated alumina, activated carbon, gypsum, tricalcium phosphate, activated soil, bauxite, magnesite, defluoron, and others. Activated alumina, activated carbon and bone char are employed most often. Each adsorbent does have advantages and limitations. Adsorption with activated alumina, for instance, is pH specific being optimum between pH 5.0 and 6.0. At pH greater than 7 silicate and hydroxide compete strongly with fluoride for active sites, and pH less than 5 lead to dissolution of activated alumina [12]. Bone char has not been accepted in some cultures due to social aspects and also the resultant organoleptic water quality and colour [13,14]. Bauxite introduces traces of aluminium in the water whereas gypsum increases the sulphate content of the water beyond WHO recommendations [4,5]. Magnesite was found to give a low sorption capacity at low and medium pH and increased pH to beyond 10 [3]. It is therefore apparent that filter identification and/or improvement in water defluoridation must be on-going. Bauxite, gypsum and magnesite have previously been researched on independently in fluoride removal from water [3,5,15]. The employment of the three materials together was thought through and tried in a composite filter prepared in a number of permutations and the ratio of their loading capacities. Batch and fixed bed configurations were attempted with the composite filter to determine optimum configuration for the filter identified. Breakthrough characteristics are particularly important in design of a fixed bed. Bed depth service time (BDST) design model and empty bed residence time (EBRT) optimisation model were employed to characterise optimum design parameters. In a fixed-bed system, the main design criterion is to predict how long the adsorbent material will be able to sustain removing a specified amount of solute from solution before breakthrough i.e. before regeneration or media replacement is needed. This period of time is called the service time of the bed. The BDST model describes a relation between the service time of the column and the depth of packed bed column. The EBRT is the time required for the liquid to fill the column, on the basis that the column does not contain adsorbent packing, and is a direct function of liquid flow rate and column bed volume. In BDST regression of bed depth and service time (time at breakthrough) were carried out where as in EBRT the adsorbent exhaustion rates were plotted against the EBRT values.

2. Results and discussion

2.1. Defluoridation kinetics

Second order kinetics were observed and the kinetic data is presented in Table 1. The equilibrium concentrations on the solid phase, q_e, obtained from the inverse of the slope compared fairly well with experimental data as demonstrated by the obtained p value of 0.4359 being much greater than 0.05. Composite materials, bauxite and gypsum appeared to lower the water pH while magnesite increased water pH. The decrease in water pH in defluoridation with bauxite and gypsum may have resulted from two attributes; firstly the amphoteric nature of oxides of aluminium and secondly the acidic behaviour of the oxides from anionic species in water, and in this case the sulphite ions. Table 2 depicts sulphite and metal oxides present in the three raw materials as obtained through X-ray fluorescence (XRF). Al_2O_3 is amphoteric as such reacts with both acids (Eq. (1)) and bases (Eq. (2)) as shown below [16];

$$Al_2O_3(s) + 6H_3O^+(aq) + 3H_2O(l) \rightarrow 2[Al(OH_2)]^{3+}(aq) \quad (1)$$

$$Al_2O_3(s) + 2OH^-(aq) + 3H_2O(l) \rightarrow 2[Al(OH)_4]^-(aq) \quad (2)$$

It has also been demonstrated through XPS analysis that the sorption of fluoride at low pH ($pH < pH_{pzc}$) for nano-AlOOH can be explained by a two step protonation/ligand exchange reaction mechanism as described through Eqs. (3) and (4).

$$\Xi Al{-}OH + H^+ \Leftrightarrow \Xi AlOH_2{}^+ \quad (3)$$

$$\Xi AlOH_2{}^+ + F^- \Leftrightarrow \Xi AlF + H_2O \quad (4)$$

This gives a net Eq. (5) below;

$$\Xi Al{-}OH_2{}^+ + H^+ + F^- \Leftrightarrow \Xi AlF + H_2O \quad (5)$$

The sorption model proposed by Eqs. (8) and (9) should result in increase in pH as there is a net removal of H^+ ions from solution. However, when initial pH is greater than the point zero charge ($pH_{pzc} = 7.8$) nano-AlOOH functions as a cation exchanger and adsorbs the sodium ions present in solution, releasing protons resulting in decrease in pH [17]. The probable mechanisms for fluoride sorption at pH > 7.8 by nano-*AlOOH* could be as shown in Eq. (6) [17].

$$AlOOH \cdot H_2O(solid) + Na^+(aq) + F^-(aq) \rightarrow AlOOH(x-1)H_2OOH^-Na^+F^-(solid) + H^+(aq) \quad (6)$$

In the present experiments the initial water pH was 8.68, fairly higher than the pH_{pzc} of AlOOH. XRF showed that the bauxite employed in these experiments contained 30.33% Al_2O_3. The decrease in pH after defluoridation with this bauxite may entail formation of AlOOH in water and subsequent protonation/ligand exchange reactions as suggested earlier [17]. The Al_2O_3 being amphoteric, may have reacted as acid in the basic water medium

Table 1
Kinetic data for bauxite, gypsum and magnesite calcined at 200 °C.

Material	Bauxite	Gypsum	Magnesite
Parameter			
k_2 (g mg^{-1} min^{-1})	4.07×10^{-2}	1.87×10^{-2}	1.59×10^{-2}
q_e kinetics (mg/g)	5.09	5.33	5.02
q_e experimental (mg/g)	5.37	5.16	4.76
R^2	0.9912	0.9891	0.9705

Table 2
Percentages of sulphites and metal oxides present in the three raw materials.

Material	Constituent			
	SO_3	Al_2O_3	CaO	MgO
Bauxite	5.18	30.33	0.76	0.56
Gypsum	34.96	2.26	28.09	1.02
Magnesite	0.51	0.51	1.89	34.57

(pH = 8.68) as illustrated earlier in Eq. (1). This lowers pH because it diminishes the OH^- concentration in water. The sorption reaction may then have occurred as per Eq. (6) enhancing the decrease in water pH.

The bauxite and gypsum contained 5.18% and 34.96% SO_3 respectively obtained through XRF analysis. It is established that covalent oxides are largely acidic. Such oxides on dissolution bind water molecules and release protons to the surrounding medium [16]. The behaviour of carbon dioxide in aqueous medium illustrates this point.

$$CO_2(g) + H_2O(l) \rightarrow [OC(OH)_2](aq) \quad (7)$$

$$[OC(OH)_2](aq) + H_2O(l) \Leftrightarrow [O_2C(OH)]^-(aq) + H_3O^+(aq) \quad (8)$$

From the foregoing reactions (Eqs. (7) and (8)) it is highly plausible that the sulphite from the bauxite and gypsum, upon entering the aqueous medium, reacted similarly as depicted below;

$$SO_3(aq) + H_2O(l) \rightarrow [O_2S(OH)_2](aq) \quad (9)$$

$$[O_2S(OH)_2](aq) + H_2O(l) \Leftrightarrow [O_3S(OH)]^-(aq) + H_3O^+(aq) \quad (10)$$

The reactions proposed in Eqs. (9) and (10) would lower pH of the water. This entails that the presence of both Al_2O_3 and SO_3 in bauxite would function in synergy for the decrease in pH in defluoridation with bauxite. This is in agreement with experimental data where defluoridation with bauxite obtained lowest pH values among the three materials. A recap of the compositional quantities of SO_3, Al_2O, CaO, and MgO in bauxite, gypsum and magnesite depicted in Table 2 shows that bauxite and gypsum contained the sulphite in greater proportions compared to magnesite as such the effect of the sulphite reactions proposed may have been negligible for magnesite. Ionic oxides being largely basic [16] will lower pH of an aqueous medium as illustrated below.

$$CaO(s) + H_2O(l) \rightarrow Ca^{2+}(aq) + 2OH^-(aq) \quad (11)$$

$$MgO(s) + H_2O(l) \rightarrow Mg^{2+}(aq) + 2OH^-(aq) \quad (12)$$

The effect of the CaO reaction may have been overshadowed by the effect of the reactions of SO_3 as proposed in Eqs. (9) and (10) resulting in a net decrease in pH in defluoridation with gypsum, SO_3 being in greater proportion to CaO in gypsum. On the other hand, magnesite having a very low content of SO_3, increased pH as effects of MgO reactions overshadowed the effect of SO_3 reactions because of the greater proportion of MgO compared to SO_3, see Table 2. From the foregoing it is plausible that defluoridation with gypsum and magnesite followed the scheme proposed in Eqs. (13) and (14), respectively;

$$CaO(s) + H_2O + F^-(aq) \rightarrow Ca(OH)F(aq) + OH^-(aq) \quad (13)$$

$$MgO(aq) + H_2O + F^- \rightarrow Mg(OH)F(aq) + OH^-(aq) \quad (14)$$

2.2. Dose and capacity

Fig. 1 depicts how the sorption capacity (mg/g) decreased with increase in dose level (g). The percentage removal however increased with increase in dose level as depicted in Fig. 2. The decrease in loading capacity with increase in level of dose is possibly a result of lower ratio of F^- ions to adsorbent mass with increase in dose, i.e. fewer fluoride ions per unit mass of adsorbent. The increase in percentage removal was possibly due to greater availability of binding sites resulting from an increase in adsorbent dose. Similar observations were made elsewhere in defluoridation experiments but with aluminium oxide hydroxide, bone char and other natural materials [17–20]. The following relations between capacity (mg/g) and dose (g), percentage removal and dose (g) were obtained from the best fit curves of the experimental data plots as shown in Table 3.

Analysis of variance indicated significant differences among mean capacities of different doses, and, significant interaction between dose and type of material. Post hoc tests showed that the mean capacity for the 0.5 g dose was significantly greater than all the means for the other doses $p < 0.05$. The mean capacity for the 1.5 g dose was significantly greater than those obtained with all doses above 1.5 g, $p < 0.05$. Means obtained for each material, when compared at $\alpha = 0.05$, were all significantly different one from the other. Mean capacity for bauxite (1.05 mg F/g) was significantly greater than the mean capacities obtained with gypsum (0.85 mg F/g) and magnesite (0.71 mg F/g), $p = 0.0252$, $p = 0.0004$, respectively. Gypsum had a significantly greater mean capacity compared to magnesite $p = 0.0052$.

2.3. Breakthrough characteristics

Greater doses obtained longer breakthrough times as shown in Fig. 3.

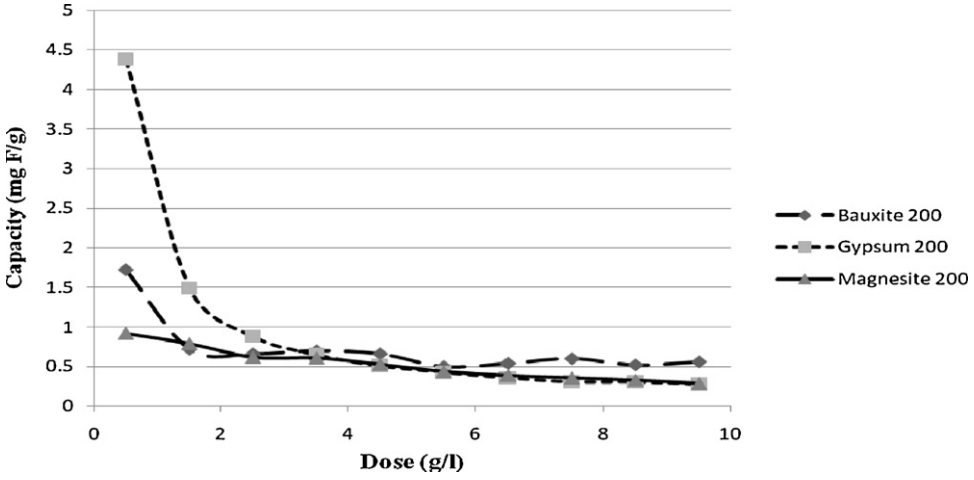

Fig. 1. Plot of sorption capacity against dose.

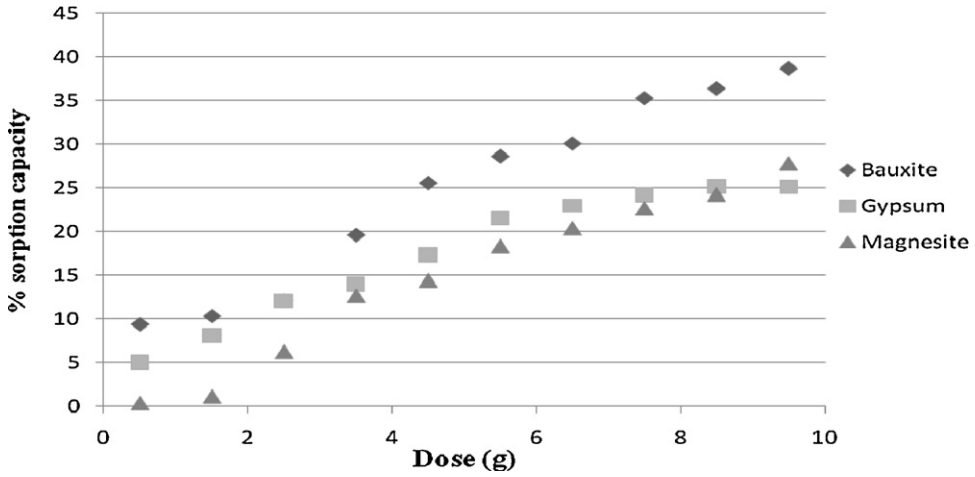

Fig. 2. Percentage removal of fluoride against dose.

Table 3
Equations for sorption relationships.

Material	Relationship between capacity (y) and dose (x)	R^2
Bauxite	$y = 1.0689x^{-0.35}$	0.8194
Gypsum	$y = 2.1796x^{-0.943}$	0.9972
Magnesite	$y = 0.0063x^2 - 0.1293x + 0.964$	0.9881
	Equation for % removal (y) and dose (x)	
Bauxite	$y = -0.119x^2 + 4.8017x + 4.5171$	0.9738
Gypsum	$y = -0.2071x^2 + 4.4426x + 2.2369$	0.9904
Magnesite	$y = -0.1488x^2 + 4.6245x - 3.33568$	0.9853

Table 4
Summary of parameters from logistic model and breakthrough curves.

	Logistics model			Breakthrough curve	
Dose (g)	k (min^{-1})	τ (min)	R^2	τ (min)	Service time t_b (min)
45	7.0×10^{-3}	55.66	0.9202	120	300
75	6.0×10^{-3}	318.98	0.9709	360	480
120	5.8×10^{-3}	370.05	0.9755	420	660
150	4.6×10^{-3}	562.17	0.9712	480	720

A comparison of the two-parameter logistic model and experimental sorption time at $C_o/2$, τ (min) revealed that the values obtained through the model were not significantly different from the values obtained from the experiments at $\alpha = 0.05$, $p = 0.83278$. Table 4 depicts data obtained from logistic model and breakthrough curve.

The operating line obtained from the EBRT optimisation model (Fig. 4) could be explained by Eq. (15);

$$\hbar = 4 \times 10^{-4}\delta - 0.0757\delta + 4.86 \quad (15)$$

In the equation, $\hbar$ is the adsorbent exhaustion rate (AER) in g/l and δ is the empty bed residence time (EBRT) in seconds. The significance of the operating line is that once the adsorbent exhaustion rate is obtained through experimentation, the respective empty bed residence time can be read-off from the operating line curve or calculated from the governing equation, the size of the column required is then determined from the empty bed residence time. Fig. 5 shows the BDST plot at 50% breakthrough. The results show that service time was directly proportional to bed depth. Earlier experiments with bone char for the sorption of cations obtained similar results [21]. The BDST parameters obtained are presented in Table 5. The critical bed depth was 7.71 cm. This entails that under the conditions of these experiments at least a bed depth of 6.56 cm is required to avoid breakthrough being obtained immediately, i.e. at time zero in the fixed bed defluoridation. The critical bed depth is one of the essential design parameters in a fixed bed.

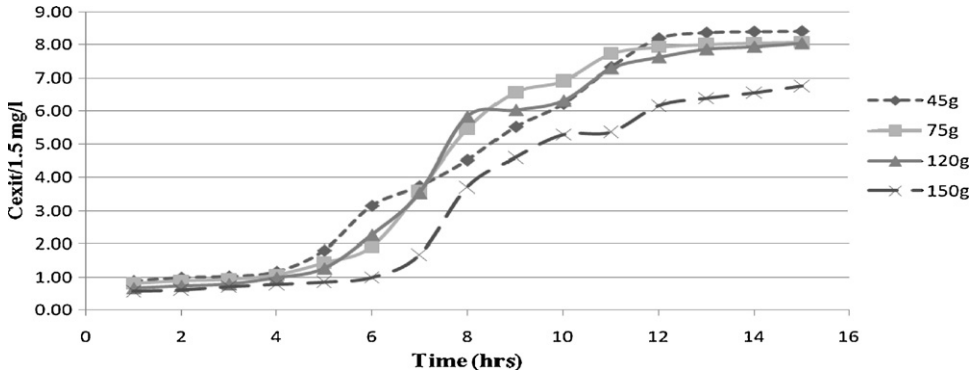

Fig. 3. Breakthrough curves for different dose levels in fixed beds.

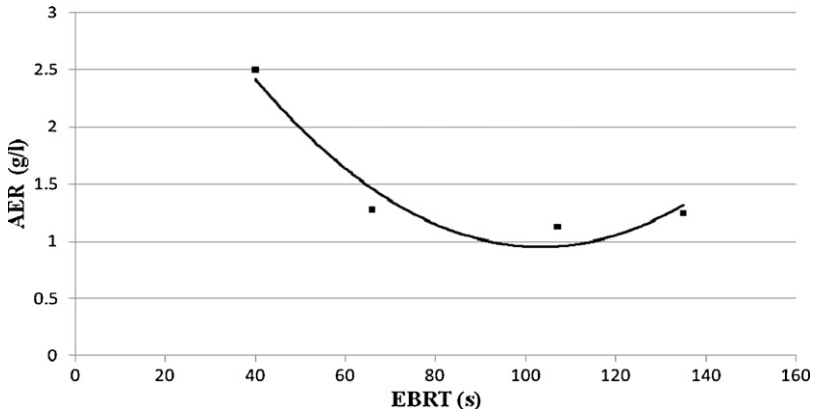

Fig. 4. Plot of adsorbent exhaustion rate (AER) against empty bed residence time (EBRT).

3. Conclusion

Second order kinetics were observed and bauxite obtained the highest while magnesite had the lowest defluoridation rate. Loading capacities (mg F^-/g) decreased while percentage sorption increased with increase in level of dose. There were significant differences in loading capacities for the nine doses experimented on, highest loading being obtainable with lowest dose and highest percentage sorption resulting from largest dose. Relationships between loading capacity (y) and dose (x) were of the form $y = Cx^{-a}$ for bauxite and gypsum but of form $y = Cx^2 - Dx + E$ for magnesite. Percentage removal of fluoride (y) and dose (x) were defined by $y = Cx^2 + Dx + E$. The constants C, D and E varied for all the three materials. Mean loading capacities were 1.05, 0.85 and 0.71 mg F^-/g. The rate constants were 4.07×10^{-2}, 1.87×10^{-2} and 1.59×10^{-2} g mg^{-1} min^{-1} for bauxite, gypsum and magnesite, respectively. A composite of the materials, prepared in the ratio of their loading capacities, obtained a critical bed depth (Z_o) of 7.71 cm and an operating line, $\hbar = 5 \times 10^{-5}\delta - 0.0113\delta + 0.929$ where $\hbar$ is the adsorbent exhaustion rate and δ is the empty bed residence time. Experimental data fitted the two-parameter logistic model fairly well as such the model is employable to defluoridation with the 200 °C-B-G-Mc filter within the context of the present research. Residual sulphate and apparent colour did not meet the WHO water quality recommendations for batch configuration; however the water quality obtained through fixed bed was within standards for apparent colour, hardness, pH, and residual concentrations of SO_4^{2-}, Al^{3+}, Fe^{2+}, and Cl^-. It is plausible that a composite defluoridation filter of calcined bauxite, gypsum and magnesite can be formulated for employment in fixed bed fluoride sorption.

Work is in progress with calcined bauxite, gypsum, magnesite and their composites with focus on effects of flow rates on breakthrough characteristics, effects of initial fluoride concentration and adsorbent particle size on loading capacity.

4. Experimental

4.1. Sorption capacity and water quality

The three materials were crushed and sieved to particle sizes of diameter 1.2–1.4 mm, activated at 200 °C for 2 h in an open air muffle furnace and then employed in batch and fixed bed defluoridation. To determine loading capacity and water quality

Table 5
Parameters obtained from the BDST plot at 50% breakthrough (C_o = 12.62, flow rate = 3.7 ml/s, particle diameter = 1.2–1.4 mm).

Parameter	Value obtained
Z_o (cm)	7.71
k (l/mg min)	6.72×10^{-4}
$\frac{N_o}{C_o v}$ (min/cm)	16.32
$-\frac{1}{kC_o}\ln\left(\frac{C_o}{C_b} - 1\right)$ (min)	125.82
R^2	0.987

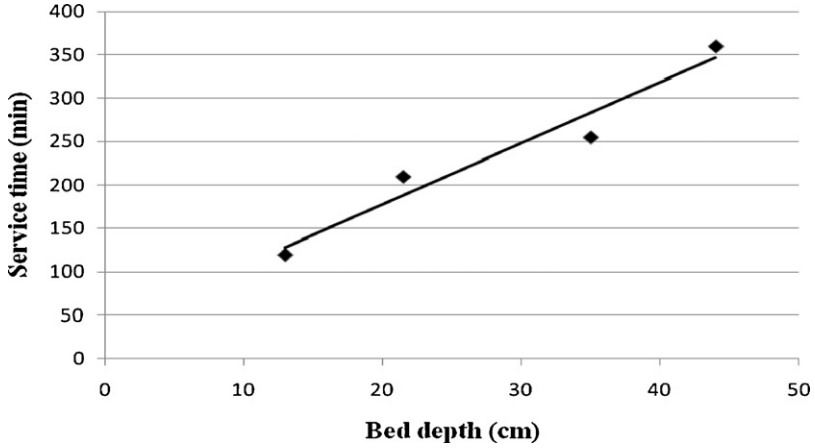

Fig. 5. Bed depth service time plot at 1.5 mg/l breakthrough.

changes in batch experiments, 1 g of each material was placed in 1 l of known fluoride concentration. The media was constantly agitated at 125 rpm. Apparent colour, pH, and concentrations of Al^{3+}, Ca^{2+}, Mg^{2+}, Fe^{2+}, $SO_4{}^{2-}$, Cl^-, and F^- were determined hourly until equilibrium fluoride concentration was obtained. The loading capacity was calculated as per Eq. (16) below;

$$q_e = \frac{(C_o - C_e)V}{m} \tag{16}$$

where q_e is the amount of adsorbed fluoride at equilibrium (mg/g); V is the volume of the solution (l); C_o and C_e are the initial fluoride concentration and fluoride concentration at equilibrium (mg/l), respectively. The term m is mass of adsorbent (g). Each experiment was replicated five times.

4.2. Defluoridation kinetics

To determine order of sorption kinetics batch experiments were carried out with the 200 °C calcines of bauxite, gypsum and magnesite. In these experiments 1 g of each material was placed in 1 l of water with a known initial fluoride concentration. The medium was agitated at 125 revolutions per minute and fluoride concentration was followed; initially every 5 min, later every 15 min and finally every 30 min, for 3 h. Adsorption kinetics was analyzed using two reaction kinetic models, pseudo first-order and pseudo second-order-equations, Eqs. (17) and (18) [22,23].

$$\ln(q_e - q_t) = \ln q_e - k_1 t \tag{17}$$

$$\frac{t}{q_t} = \frac{1}{k_2 qe^2} + \frac{1}{q_e} t \tag{18}$$

The terms q_e and q_t are equilibrium concentration and concentration at time t, and k_1, k_2 are rate constants for the first and second order kinetics, respectively. In examining fitness for first order kinetics $\ln(q_e - q_t)$ was plotted against t, and, in determining fitness for second order kinetics t/q_t was regressed against t. The rate constants k_1 and k_2 were calculated from the slope and intercept of the regression curves, respectively.

4.3. Breakthrough characteristics

Fixed bed experiments were carried out with masses (column heights) of 45 g (13 cm), 75 g (21.5 cm), 120 g (35 cm) and 150 g (44 cm) of composite bauxite:gypsum:magnesite mixed in the ratio of their optimum loading capacities. Apparent colour, pH, and concentrations of Al^{3+}, Ca^{2+}, Mg^{2+}, Fe^{2+}, $SO_4{}^{2-}$, Cl^-, and F^- were determined hourly until equilibrium fluoride concentration was obtained. Bed depth was regressed with service time and adsorbent exhaustion rate (AER) was plotted against empty bed residence time (EBRT). EBRT is time taken to fill the column volume with water when it is not packed with adsorbent. The BDST equation (19) below was employed in characterising fixed bed defluoridation;

$$t = \frac{N_o Z}{C_o \nu} - \frac{1}{kC_o} \ln\left(\frac{C_o}{C_b} - 1\right) \tag{19}$$

where t is service time/operating time of bed (min) before breakthrough, N_o is volumetric sorption capacity of bed (mg/l), Z is bed depth (cm), C_o is initial solute concentration (mg/l), ν is velocity (ml/s), k is kinetic rate parameter (l/mg h), and C_b is breakthrough solute concentration (mg/l). The service time was then plotted against bed depth and Z_o, critical bed depth, was obtained as the Z value at $t = 0$ (x-intercept). The slope obtained equalled the value of $N_o/C_o\nu$ and the y-intercept gave the value of $-1/kC_o\ln(C_o/C_b - 1)$. Adsorbent exhaustion rate (AER), calculated through dividing mass of adsorbent by volume of treated water, was plotted against empty bed residence time (EBRT). The value of $N_o/C_o\nu$ is time required to exhaust a unit length of sorbent in column under test conditions whereas $-1/kC_o\ln(C_o/C_b - 1)$ gives the time required for an adsorption wave front to pass through the critical bed depth, Z_o. The critical bed depth is the minimum bed depth that can be employed in a sorption column and not result in instant breakthrough concentrations i.e. exit concentration (C_{exit}) being equal to inlet concentration (C_{inlet}) at $t = 0$. The plot of AER against EBRT yields operating line [24]. This is the curve that is indicative of possible optimum for AER with respect to size of column. When the AER is very high the EBRT must be low entailing a small column. This is a case of high operating cost, as the bed material must be changed within short operating times, and low capital cost, because of the small column required [25]. Conversely a big column, entailing high EBRT, requires low AER. Two parameter logistic model was employed to further characterise breakthrough in fixed beds. This logistic model has been employed before in modelling defluoridation breakthrough characteristics in fixed beds albeit with surface-tailored zeolite [26].

The two parameter logistic model, employed to further characterise breakthrough, is governed by Eq. (20) below;

$$\ln\left(\frac{C_t}{C_o - C_t}\right) = k(t - \tau) \tag{20}$$

where k (min^{-1}) is rate constant and a measure of the slope of the breakthrough curve (BTC). Steeper BTCs have larger k values. The unit τ (min), is time at which exit stream concentration is 50% that of the inlet stream. C_t (mg/l) is concentration at time t, C_o (mg/l) is initial concentration. Through the plotting of $\ln(C_t/(C_o - C_t)$ against time (t), k and τ were obtained as slope and intercept, respectively.

Acknowledgements

The author acknowledges the financial support received from Malawi Government. The sponsors did not have any involvement in the research design, execution and data analysis nor in the preparation and submission of this paper.

References

[1] B.K. Shrivastava, A. Vani, Asian J. Exp. Sci. 23 (2009) 269–274.
[2] V.S. Vaiss, R.A. Berg, A.R. Ferreira, I. Borges Jr., A.A. Leitão, J. Phys. Chem. A 113 (2009) 6494–6499.
[3] J.J. Singano, Investigation of the mechanisms of defluoridation of drinking water by using locally available magnesite, Ph.D. thesis, University of Dares Salaam, 2000.
[4] S.M.I. Sajidu, W.R.L. Masamba, B. Thole, J.F. Mwatseteza, Int. J. Phys. Sci. 3 (2008) 1–11.
[5] B. Thole. Water defluoridation with Malawi bauxite, gypsum and synthetic hydroxyapatite, bone and clay: effects of pH, temperature, sulphate, chloride, phosphate, nitrate, carbonate, sodium potassium and calcium ions, M.Sc. thesis, University of Malawi, 2005.
[6] S.K. Nath, R.K. Dutta, Indian J. Chem. Technol. 3 (2010) 120–125.
[7] H.X. Wu, T.J. Wang, L. Chen, Y. Jin, Ind. Eng. Chem. Res. 48 (2009) 4530–4534.
[8] S. Ayoob, A.K. Gupta, P.B. Bhakat, Chem. Eng. J. 140 (2008) 6–14.
[9] G. Ghiglieri, R. Balia, G. Oggiano, D. Pittalis, Hydrol. Earth Syst. Sci. Discuss. 6 (2009) 7321–7348. http://www.hydrol-earth-syst-sci-discuss.net/6/7321/2009/.
[10] A. Dysart, Investigation of defluoridation options for rural and remote communities, Research Report No. 41, The Cooperative Research Centre for Water Quality and Treatment, Salisbury SA 5108, Australia, 2008.
[11] E.J. Ncube, C.F. Schutte, Water SA 31 (2005) 35–40.
[12] R.C. Meenakshi, Maheswari, J. Hazard. Mater. B137 (2006) 456–463.
[13] H. Mjengera, Optimisation of bone char filter column for defluoridating drinking water at household level in Tanzania, Ph.D. thesis, University of Dares Salaam, 2002.
[14] M. Kongpun, Defluoridation and Economic Efficiency among Anionic Exchange Resin and Precipitation Accelerated by Bone Char and Activated Carbon, Fluoride Research Laboratory – Intercountry Centre for Oral Health (ICOH), Thailand, 200.1
[15] K.H. Peter, J. Eng. Appl. Sci. 4 (2009) 240–246.
[16] D.F. Shriver, P.W. Atkins, C.H. Langford, Inorganic Chemistry, second ed., ELBS, Oxford University Press, 1994.
[17] S.G. Wang, Y. Ma, Y.J. Shi, W.X. Gong, J. Chem. Technol. Biotechnol. 83 (2009) 1043–1050.

[18] CDN (Catholic Diocese of Nakuru), K. Muller, CDN's defluoridation experiences on a community scale. Reviewed by P. Jacobsen, CDN and Swiss Federal Institute of Aquatic Science and Technology, Eawag, 2007.
[19] N. Viswanathan, S. Meenakshi, J. Appl. Polym. Sci. 112 (2009) 1114–1121.
[20] S. Chidambaram, A.L. Ramanathan, S. Vasudevan, Water SA 29 (2003) 339–344.
[21] D.C.K. Ko, J.F. Porter, G. McKay, Ind. Eng. Chem. Res. 38 (1999) 4868–4877.
[22] L. Lv, J. He, M. Wei, X. Duan, Ind. Eng. Chem. Res. 45 (2006) 8623–8628.
[23] M. Sarkar, A. Banerjee, P.P. Pramanick, Ind. Eng. Chem. Res. 45 (2006) 5920–5927.
[24] E.M. Damte, Removal of fluoride from water using granular aluminium hydroxide: adsorption in a fixed bed column. M.Sc. thesis, Addis Ababa University, Ethiopia, 2006.
[25] M.M. Emamjomeh, M. Sivakumar, J. Environ. Manage. 90 (2009) 1204–1212.
[26] M.S. Onyango, T.Y. Leswifi, A. Ochieng, D. Kuchar, F.O. Otieno, H. Matsuda, Ind. Eng. Chem. Res. 48 (2009) 931–937.